Journal of Environmental Chemical Engineering 13 (2025) 117710

Contents lists available at ScienceDirect

Journal of Environmental Chemical Engineering

journal homepage: www.elsevier.com/locate/jece

Hydrothermal treatment of contaminated sorghum: Hydrochar properties and characterization/phytotoxicity evaluation of the liquid phase

Karima Mehrez [a,d,*], Lydia Fryda [a], Hayet Djelal [a], Mathilde Mercier [a], Heather Wray [b], Abdoulaye Kane [a], Nathalie Leblanc [c], Rian Visser [b]

[a] Unilasalle-Ecole des Métiers de l'Environnement, CYCLANN, Campus de Ker Lann, Bruz 35170, France
[b] Netherlands Organization for Applied Scientific Research TNO, Petten 1755 LE, the Netherlands
[c] UniLaSalle, Université d'Artois, EA7519 Transformation & Agro-Ressources, Mont-Saint-Aignan 76130, France
[d] University of Rouen Normandy, Rouen 76000, France

ARTICLE INFO

Keywords:
Contaminated sorghum
Heavy metals
Hydrochar
Hydrothermal carbonization
Liquid phase
Parametric study

ABSTRACT

Reducing the heavy metals (HMs) content and enhancing the fuel quality of phytoremediation biomass is a crucial environmental and technical challenge. This study investigates hydrothermal carbonization (HTC) as a promising way to recycle HMs-contaminated sorghum (CS) into a cleaner solid biofuel and characterize and evaluate the liquid by-product more deeply. A systematic study of temperature (180–240°C) and residence time (0.5–4 h) revealed that the hydrochar higher heating value increases with temperature (from 20.6MJ/kg to 25.5MJ/kg), albeit reducing the solid yield (down to 62 % from 80 %). HC200–0.5 was identified as the optimum best among the tested experimental conditions regarding the application of hydrochar as solid biofuel with respect to energy content and reduced HMs content. The low pH (3.96 ± 0.08) of the effluents due to the high concentration of carboxylic acids (up to 50 %), and the high total organic carbon (TOC) and HMs content are accountable for the strong phytotoxicity, as revealed by the complete inhibition of seed germination. These findings underline the necessity of post-treatment strategies for HTC effluents. This work puts emphasis on hydrochar quality and at the same time addresses the composition of the liquid phase and its toxicity, an aspect often neglected in the literature, proposing an integrated process to valorize HMs contaminated lignocellulosic biomass, retaining the contamination in the effluents that need to undergo adapted treatment.

1. Introduction

The accumulation of heavy metals (HMs) in soil and water poses a risk to the environment and human health [1]. Iron (Fe), manganese (Mn), copper (Cu), zinc (Zn) and nickel (Ni) are essential HMs that living organisms need in small quantities for their vital physiological and biochemical functions [2]. In contrast, non-essential HMs such as cadmium (Cd), lead (Pb), arsenic (As), mercury (Hg) and chromium (Cr) are not required by living organisms for any of their functions [3]. The most toxic HMs and metalloids include Cr, Ni, Cu, Zn, Cd, Pb, Hg and As [4]. Phytoremediation by hyperaccumulator plants is one of the methods to decontaminate soils and waters contaminated by HMs, while increasing bacterial diversity in soils. The hyperaccumulator plants can store HMs in different parts such as roots, stems, leaves and flowers, for example *Helianthus annuus* that can accumulate 107.7 mg/kg of Pb and 71.3 mg/kg of Cd in its roots [5]. *Miscanthus x giganteus* considered as a potential hyperaccumulator of HMs from polluted sites, it can accumulate 529.8 mg/kg, 365.8 mg/kg and 30.8 mg/kg of Pb, Zn and Cd, respectively [6]. Gorelova et al. found that the root of Sorghum bicolor can accumulate 96100 mg/kg of Fe, 1780 mg/kg of Mn, 45.5 mg/kg of V and 16 mg/kg of Cr [7]. However, the significant volumes of HMs rich biomass produced may be again a risk to the environment if not managed properly [8]. The natural decomposition of this contaminated biomass brings along the risk of release of HMs in the environment. There are several thermochemical processes that can convert contaminated biomass to energy or functional value-added material such as combustion, pyrolysis and gasification, which can control and limit the release of HMs to the environment [9].

Hydrothermal carbonization (HTC) is a thermochemical process that can be considered as a pretreatment and washing step of the contaminated biomass [10]. HTC takes place in an aqueous medium heated to sub-critical temperatures (180–250°C), under self-generated pressure

* Corresponding author at: Unilasalle-Ecole des Métiers de l'Environnement, CYCLANN, Campus de Ker Lann, Bruz 35170, France.
E-mail address: karima.mehrez@unilasalle.fr (K. Mehrez).

https://doi.org/10.1016/j.jece.2025.117710
Received 7 March 2025; Received in revised form 12 May 2025; Accepted 22 June 2025
Available online 23 June 2025

[11]. This process converts biomass and organic waste into solid biofuel, liquid effluents, and gas. Hydrochar is a solid biofuel with enhanced properties compared to raw biomass, particularly in terms of material structure, heating value and thermal stability [12]. The process ca be enhanced by modifying the operational conditions, for example the addition of 0.2 mol/L of H_2SO_4 during the HTC of grass leaves enhanced the hydrochar's thermal stability, degree of carbonization, higher heating value, and energy densification [13]. Hydrochar can be utilized either independently or blended with other fuels in energy production systems [14].

Literature suggests that the transfer of HMs present in the contaminated biomass can migrate to the liquid phase of HTC, rendering HTC a pretreatment and washing step of contaminated biomass [15]. Assuming that the HTC process can be controlled in such a way that the contaminants can be transferred into an easier to manage effluent, this will reduce the need to handle large volumes of contaminated lignocellulosic biomass and offer the possibility to valorize it in conventional ways, minimizing the risk of potential release of the contamination back into the environment [9]. Zhang et al. successfully removed 95 % of Cd and 89.3 % of Zn from a Cd/Zn hyperaccumulator (*Sedum alfredii)* under HTC conditions at 210°C with the addition of 0.2 M HCl. The resulting hydrochar can be utilized both as a solid fuel and an adsorbent. When it was tested for Cu adsorption, it achieved 73.3 % of its equilibrium sorption capacity within one hour [16].

The liquid phase generated during HTC of HMs contaminated biomass is a potential source of environmental toxicity. This aqueous phase contains not only organic compounds from the thermochemical degradation of lignocellulosic biomass (organic acids, phenols, furfurals, etc.), but also a considerable proportion of the HMs initially present in the raw material. These metals, solubilized in ionic or complex form, can pose a high risk to aquatic ecosystems if not properly treated [17]. In addition, the presence of organic matter (humic and fluvic acids) and HMs can form organometallic complexes [18]. These complexes can have synergistic toxic effects, affect aquatic wildlife and disrupt food chains [19]. Several review articles on HMs migration during HTC highlight the need for post-treatment of the liquid phase, such as extraction, ion exchange, or precipitation [20–23]. Therefore, proper management and treatment of this by-product is essential to ensure the sustainability of the HTC process, particularly when applied to contaminated biomass.

Sorghum harvested from a site contaminated with HMs, was subjected to lab-scale HTC at various temperatures between 180 and 240°C, and for varying contact times, 0.5–4 h at 200°C. The dual focus of the present study is to identify the optimal operating conditions of HTC of HMs contaminated sorghum aiming to maximize the transfer of HMs from the biomass to the liquid phase, and on the characterization of the products in order to assess the potential of hydrochar as a solid biofuel. The novelty of the work is the comprehensive integration of contaminated biomass HTC conversion, in depth hydrochar and effluents evaluation by thorough characterizations including a phytotoxicity analysis and proposing common technologies for treating the effluents.

2. Materials and methods

2.1. Biomass: Sorghum

Sorghum (CS) was collected from long-term contaminated area, located in Thorikon of Lavreotiki peninsula (SE of Attica, 37°43'59''N,24°02'40''E, 5 m a.s.l.), at 3 km from the city of Lavrion, Greece. Between the late classical and early Hellenistic periods, the area developed into a state-run ore processing industry, significantly impacting the environment through the generation of various mining wastes (tailings, slag, litharge). Modern mining (1864–1982 AD) further contaminated soils with toxic elements Pb, Cd. Over time, an estimated 2.26 million tons of lead and 4500 tons of silver were produced, with 4.3 million tons of excavated material left exposed to erosion [24]. The CS particle size is 1–3 mm. Table 1 shows the concentration of heavy metals in the contaminated sorghum.

2.2. Hydrothermal carbonization processes and products analysis/ characterization

2.2.1. Hydrothermal carbonization processes description

All the experiments were carried out in a hydrothermal installation which is composed of two main parts; the controller which is of the brand «EQUILABO, Rillieux la pape, France» and the hydrothermal reactor of the brand PARR Instrument Company, Series 4621 stainless steel, Moline, Illinois USA" with a total capacity of 1 L, inside diameter of 10 cm and a height of 14.5 cm. Hydrothermal carbonization experiments of CS were carried out at 4 temperatures: 180, 200, 220 and 240°C, for an exposure time of 0.5 h and at 200°C for an exposure time of 2 h and 4 h. 60 g of CS and a volume of distillated water of 600 mL corresponding to a biomass/water ratio of 1/10 are introduced into the hydrothermal reactor so that the reactor was filled to 2/3 of its volume. After completion of the experiments, the reactor gradually cooled down to room temperature. The hydrochars were separated from the liquid phase by centrifugation (ThermoFisher Scientific HERAEUS MEGAFUGE, Osterode am Harz, Germany) for 10 min at 20°C and 5000 rpm. The hydrochars were washed 3 times with 700 mL of distilled water then dried (VWR DRY-Line, Leicestershire, UK) at 105°C to constant weight then ground to fine particles and sieved. The liquid phase was stored at 4°C. Each HTC experiment was conducted twice.

2.2.2. Chemical analysis and products characterization

- Hydrochar characterization

HC is used throughout the study as an abbreviation for hydrochar. The elemental analysis of CS and HC was performed by an CHNS-O Analyzer, Flash 2000, Thermo Fisher scientific, Bremen, Germany. The higher heating value (HHV) was determined in a Parr 6400 bomb calorimeter (Parr Instrument company, Moline, USA). HMs concentrations were quantified by inductively coupled plasma mass spectrometry (ICP-MS) (Agilent technologies 7700, USA). The destruction of the samples was done according to the standards NEN-EN-ISO 16967_2015 EN Macro and NEN-EN-ISO 16968_2015 EN Minor and the measurement was done using the NEN6966 standard. Fourier Transform Infrared spectrometer (JASCO FT/IR-4X spectrometer, Tokyo, Japan) was employed for the analysis of the functional groups on the hydrochar surface. The absorbance values range for the samples was 4000–500 cm^{-1}. The surface morphology was observed by a scanning electron microscopy (JEOL SEM, JSM-IT100, Tokyo, Japan). The HCs samples were placed in an oven (Thermolyne, Thermo Fischer scientific, Asheville USA) at 550°C to determine the ash content following the standard NF T90–029.

Table 1
Characterization of sorghum.

Ash (% dry wt.)	7 ± 0.05
Humidity (%)	13.0 ± 0.74
HHV (MJ/kg)	19.9 ± 0.95
C (% dry wt.)	49.3 ± 5.34
H (% dry wt.)	5.8 ± 0.05
N (% dry wt.)	1.1 ± 0.14
O (% dry wt.)	41.8 ± 1.32
Heavy metals (mg/kg)	
Al	1363 ± 209.35
Cd	21 ± 1.06
Fe	958 ± 166.20
Mn	66 ± 2.02
Ni	6.33 ± 0.88
Pb	228 ± 29.80
Zn	321 ± 20.02

The HC yield, Ash content and the energy yield of HC are calculated as follow [25,26]:

$$HC\ yield(\%) = \frac{dw_{(HC)}}{dw_{(CS)}} \times 100 \quad (1)$$

Where: $dw_{(HC)}$: dry weight of HC (g); $dw_{(CS)}$: dry weight of contaminated sorghum (g).

$$Ash\ content = \frac{Ash\ weight}{dw_{(HC)}} \times 100 \quad (2)$$

$$Energy\ yield(\%) = HC\ yield(\%) \times ED \quad (3)$$

Where ED: energy densification ratio and is calculated as follows:

$$ED = \frac{HHV_{(HC)}}{HHV_{(CS)}} \quad (4)$$

Where: $HHV_{(HC)}$: higher heating value of HC (MJ/kg); $HHV_{(CS)}$: higher heating value of contaminated sorghum (MJ/kg).

Thermogravimetric analysis was conducted in a NETZSCH TG209 F1 thermogravimetric analyzer (Selb, Germany) to study the combustion behavior of CS and hydrochars. Approximately 8 mg CS and hydrochars samples, were placed in an Al_2O_3 crucible. The samples were exposed to a 50 mL/min flow of air (STP) as the carrier gas and heated from 25°C to 800°C at a rate of 10 °C/min. To evaluate the combustion characteristics of CS and hydrochars, the comprehensive combustibility index (CCI), ignition index (Di), flammability index (F) and ΔT were calculated by the follow equations based on previous studies [27,28].

$$CCI = \frac{DTG_{max} \times DTG_{mean}}{T_i^2 \times T_b} \quad (5)$$

$$Di = \frac{DTG_{max}}{T_i \times T_b} \quad (6)$$

$$F = \frac{DTG_{max}}{T_i^2} \quad (7)$$

With: DTG_{max} and DTG_{mean} represent the maximum and average derivative weight loss rates (%/min), respectively. T_i and T_b were the ignition and the burnout temperatures (°C), respectively. T_i was determined based on the temperature at which the DTG curve (the first derivative of TG curve) reached its peak value, along with the corresponding slope at the intersection with the TG profile. T_b was identified based on the point of mass stabilization [27,29].

$$\Delta T = T_b - T_i \quad (8)$$

The heavy metals removal efficiency from CS is calculated as follows:

$$heavy\ metals\ removal\ efficiency(\%) = 100 - \left(\frac{[HMs]_{HC}}{[HMs]_{CS}} \times HC\ yield\right) \quad (9)$$

With: $[HMs]_{CS}$: the heavy metals concentration in contaminated sorghum (mg/kg).

$[HMs]_{HC}$: the heavy metals concentration in hydrochar (mg/kg).

Liquid phase characterization

The abbreviation Lp is used throughout the study for Liquid phase. The pH and the conductivity of the Lp were measured by a pHmeter (WTW, pH3110, Weilheim, Germany) and a Conductivity meter (WTW, Cond 3110, Weilheim, Germany), respectively. Before each analysis, the liquid was filtered using a syringe filter (sartorius, 0.45 μm, Goettingen, Germany). Organic acid concentrations were determined using an ion chromatograph (ICS-2100, Thermo Fisher Scientific, Waltham, USA) equipped with a Vanquish Diode Array Detector (VH-D10-A). The eluent consisted of Milli-Q water produced by a Reference Millipore system. Hydroxide ions were generated in situ using a Thermo/Dionex EGC III KOH eluent generator cartridge. Gradient hydroxide eluant was used: 1 mM for 0–8 min; 30 mM for 8–30 min and 1 mM for 30–35 min. The chromatographic conditions were as follows: flow rate of 1.5 mL/min, injection volume of 25 μL, and an isothermal column temperature of 30°C. The separation was performed using a Thermo AS11-HC analytical column. The analysis of the aldehydes, ketones, alcohols and phenol concentration was performed by an UHPLC (Thermo Fisher Scientific, Vanquish UHPLC System, Vanquish Diode Array Detector VH-D10-A, Germering, Germany) with a mobile phase consisting of 0.05 % v/v formic acid (A)-Acetonitrile (B) and the gradient program was set as follows: 0–12 min: 90–10 % (B); 12–25 min: 85–15 % (B); 25–35 min: 57–25 % (B); 35–46 min: 25–75 % (B) and 46–51 min: 90–10 % (B). Flow rate: 1 mL/min. The injected volume: 5 μL; Column temperature: 30°C; Type of column used: Accucore C30 150 mm*4.6 mm particle size 2.6 μm. The amount of organic matter in the liquid phase samples was determined using a Total Organic Carbon (TOC) analyzer (SHIMADZU TOC-L, Kyoto, Japan). The liquid phase was filtered using 0.45 μm syringe filters (Sartorius, Göttingen, Germany). The analysis conditions were as follows: injection volume of 150 μL, acidification using 2 N HCl and 25 % H_3PO_4, and a combustion column temperature of 680°C. HMs concentrations were quantified using the inductively coupled plasma atomic emission spectroscopy (ICP-AES) (Thermo scientific ICAP 6200 duo, Bremen, Germany). To measure the dry weight of the HTC liquid phase (Lp), 5 mL of liquid sample was placed in the oven (VWR DRY-Line, Leicestershire, UK) at 105°C to constant weight. The dry weight ($dw_{(Lp)}$) and yield of HTC Lp are calculated as follows:

$$dw_{(Lp)} = \frac{V_{Tot} \times m}{5} \quad (9)$$

Where: V_{Tot}: the total volume of the HTC Lp (mL); m: the dry weight of the 5 mL of the HTC Lp (g); $dw_{(Lp)}$: dry weight of HTC Lp (g).

$$Lp\ yield(\%) = \frac{dw_{(Lp)}}{dw_{(CS)}} \times 100 \quad (10)$$

Gas yield was calculated as follows:

$$Gas\ yield(\%) = 100 - (HC\ yield + Lp\ yield) \quad (11)$$

To evaluate the phytotoxicity of the HTC liquid phase, germination tests were performed. Samples of 5 mL volume of the HTC liquid phase, both undiluted and at three dilution levels (1:2, 1:5, and 1:10 with osmosis water), were added to Petri dishes (diameter 10 cm) lined with filter paper. 10 *Alenois cress* seeds, sourced from a farm in Saint Marthe, France, were placed equidistantly in each dish. Osmosis water was used as a control under the same conditions. All Petri dishes were then incubated at 25 °C for 48 h in darkness. Germination was defined as the emergence of a visible root from the seed.

The germination index (GI) was calculated as follows:

$$GI(\%) = \frac{Seed\ germination(\%) \times Root\ length\ of\ seed\ sample}{Seed\ germination(\%) \times Root\ length\ of\ seed\ control} \times 100 \quad (12)$$

3. Results and discussion

3.1. Mass balance results

Fig. 1 shows the mass yields of the products (hydrochar, liquid phase and gas) of the hydrothermal carbonisation of the contaminated sorghum (CS) at different temperatures (180, 200, 220 and 240°C) for one exposure time of 0.5 h, and the mass yields of HTC products for 3 exposure times at 200°C.

The increase in temperature led to a decrease in the mass yields of HCs from 80.28 % at 180°C to 62.37 % at 240°C. The initial phase of the hydrothermal reactions involves hydrolysis, where water interacts with the lignocellulosic biomass components [30]. Hydrolysis results in the formation of a mixture of soluble organic substances and carbon-rich solids [31]. As the temperature raised to 220°C and 240°C, partial

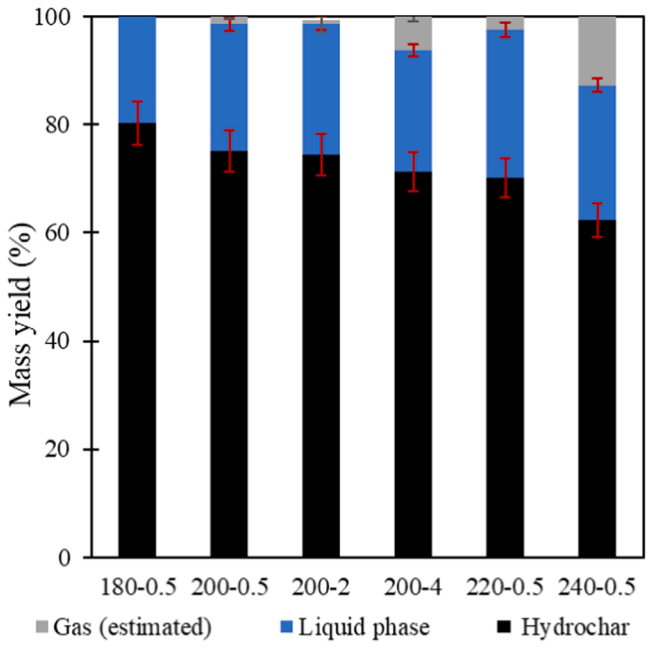

Fig. 1. Influence of temperature and exposure time on the mass yield of HTC products (% Gas is estimated).

gasification of the char takes place, resulting in a decrease in the HC yields while gas forms due to the acceleration of dehydration and decarboxylation reactions [32]. Relative to temperature, exposure time had a similar effect on solid product recovery but to a smaller degree: the solid hydrochar yield was highest at shorter exposure times (75.11 % at 0.5 h) and decreased at longer exposure times (71.42 % at 4 h).

3.2. Elemental analysis, calorific value of hydrochars and energy balance

To assess the characteristics and composition of hydrothermally treated contaminated sorghum, and evaluate its suitability as solid fuel, carbon (C), hydrogen (H), oxygen (O) and nitrogen (N), were determined, along with the higher heating value (HHV). Additionally, energy densification and energy yield were calculated. The results are shown in Table 2. The HHV of the HCs increased from 20.2MJ/kg to 25.2MJ/kg with the temperature rise from 180°C to 240°C. These values are comparable and higher to lignite coal, which exhibits an HHV of 16 MJ/kg [33]. The increase in HHV of HC is related to their carbon content which increases from 49.1 % to 60.5 %. As seen in Table 2, the ash content of HC varies between 3 % and 4 %, which is lower compared to the ash content of untreated CS (7 %). This is due to the fact that part of the inorganic matter of the sorghum leaches out towards the liquid phase [34].

The energy densification ratio rises from 1.01 to 1.26 with the increase of the reaction temperature from 180 to 240°C. This ratio reflects the increased energy content of the HC relative to the fresh sorghum [35]. Despite the enhancement of the HHV of HCs by HTC due to the increasing of carbon content, raising the reaction temperature during HTC elevates the energy costs of HTC. In contrast to the HHV and energy densification ratio, the energy yield slightly decreased from 81 % to 78 % at 180°C and 240°C, respectively, due to the reduction in mass yield. All the HC show a significant energy yield. However, higher temperatures lead to mass loss and increased energy consumption, making it more suitable to perform HTC at 180°C or 200°C rather than at 240°C.

The H/C and O/C ratios are essential criteria for estimating the degree of deoxygenation and the content of aromatic compounds during hydrothermal carbonization (HTC) of biomass. A higher H/C ratio suggests a lower aromatic content in HC [36]. The H/C and O/C ratios decrease as the temperature or exposure time increases for all HCs, as shown in Fig. 2. This variation in ratios can also reveal reaction pathways: dehydration (H_2O production) and decarboxylation (production of CO_2 or carbonyl compounds, including carboxylic acids) during the HTC [37]. HC 240°C-0.5 h has the best H/C and O/C ratio compared with other HCs. Based on the diagram of Van Krevelen, the HC 240°C-0.5 h hydrochar is very similar to lignite (HHV=15–20MJ/kg), based on this comparison it may be considered as a potential solid biofuel [38].

3.3. Thermogravimetric analysis and combustion evaluation of hydrochars

To better evaluate if the quality of CS hydrochars matches the solid biofuel demands, a thermogravimetric analysis was performed to study their combustion behavior. TG analysis provided insights into the combustion behavior of the samples, as shown in Fig. 3. Based on the TG curves, four stages of mass loss were identified: stage 1 water evaporation; stage 2 release and combustion of volatiles associated with the first peak in the DTG curves; stage 3 combustion of fixed carbon corresponding to the second DTG peak; and stage 4 continued combustion of minor amounts of fixed carbon and decomposition of inorganic matter [26].

The HC exhibited sharper and more pronounced peaks at the second stage compared to CS. The TG curve shows a significant mass loss for the CS, which reflects its higher volatile content. In contrast, the HC exhibited increased mass loss regions during the third stage, indicating a rather complete combustion of the fixed carbon [39]. The DTG curves show that hydrochars HC 180–0.5, HC 200–0.5, HC 220–0.5, and HC 240–0.5 reach their DTG_{max} at 304°C (-49.24 %.min^{-1}), 298°C (-57.56 %.min^{-1}), 301°C (-28.73 %.min^{-1}) and 275°C (-13.73 %.min^{-1}), respectively. This decrease observed for HC can be explained by the destruction of cellulose and hemicellulose still present in HC during the HTC process [40]. Table 3 summarizes the combustion parameters of CS and HC, including the ignition temperature (T_i), burnout temperature (T_b), ΔT, the comprehensive combustibility index (CCI), ignition index (Di) and flammability index (F).

The values of the Ti temperature for hydrochars (HC180–0.5, HC200–0.5, HC220–0.5 and HC240–0.5) remain constant around approximately 290°C. The hydrochar HC 200–0.5 exhibits a Tb

Table 2
Characteristics of hydrochar produced at different HTC temperature and exposure time.

	HC 180–0.5	HC 200–0.5	HC 220–0.5	HC 240–0.5	HC 200–2	HC 200–4
Ash (% dry wt.)	3.6 ± 0.34	3.8 ± 0.14	3.5 ± 0.54	3.6 ± 0.24	4.3 ± 0.31	4.0 ± 0.16
Humidity (%)	5.4 ± 0.53	4.2 ± 0.39	3.6 ± 2.87	2.4 ± 0.88	4.4 ± 0.69	3.8 ± 2.45
HHV (MJ/kg)	20.2 ± 0.41	21.4 ± 0.41	22.7 ± 0.22	25.2 ± 0.33	21.4 ± 0.72	21.5 ± 1.19
C (% dry wt.)	49.1 ± 0.62	53.4 ± 0.22	55.6 ± 0.47	60.5 ± 1.13	54.4 ± 0.11	56.2 ± 0.25
H (% dry wt.)	6.1 ± 0.30	5.9 ± 0.05	5.7 ± 0.04	5.8 ± 0.01	5.8 ± 0.07	5.5 ± 0.13
N (% dry wt.)	1.1 ± 0.00	1.1 ± 0.00	1.2 ± 0.00	1.4 ± 0.04	1.1 ± 0.02	1.1 ± 0.11
O (% dry wt.)	37.1 ± 1.23	34.4 ± 0.67	31.6 ± 0.06	26.1 ± 0.26	32.9 ± 0.27	36.2 ± 4.32
Energy yield (%)	81.4 ± 4.35	80.6 ± 0.54	79.9 ± 2.52	78.8 ± 2.86	79.9 ± 1.25	77.0 ± 1.25
Energy densification	1.01 ± 0.02	1.07 ± 0.02	1.13 ± 0.01	1.26 ± 0.01	1.07 ± 0.03	1.08 ± 0.05

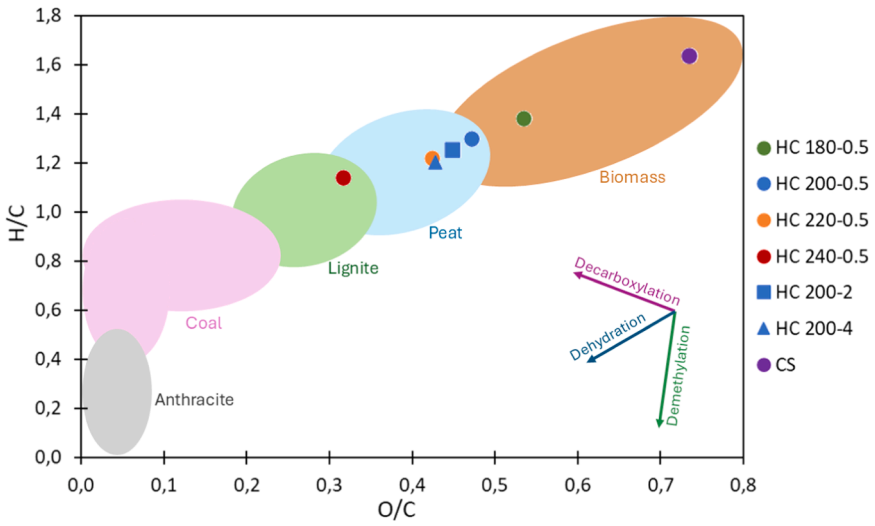

Fig. 2. Van Krevelen diagram of contaminated sorghum (CS) and hydrochars.

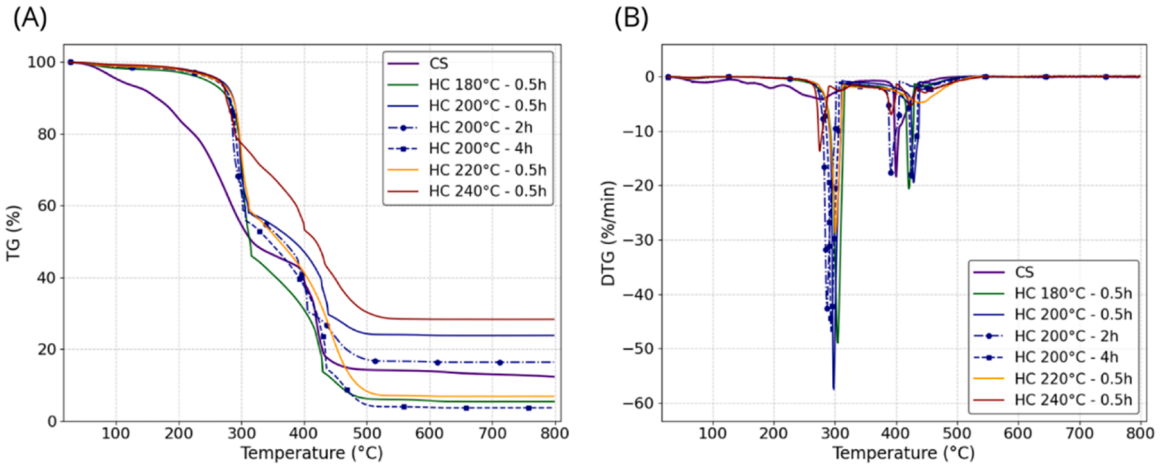

Fig. 3. TG(A)-DTG(B) curves of CS and hydrochars: temperature and exposure time effect.

Table 3
Combustion characteristics parameters of CS and hydrochars.

Sample	Residual mass (%)	DTG_{max} (%/min)	DTG_{mean} (%/min)	T_i (°C)	T_b (°C)	ΔT (°C)	CCI (10^{-7} ($\%^2$.min^{-2}.°C^{-3})	Di ($10^{-4\%}$.min^{-1}.°C^{-2})	F (10^{-4} %.min^{-1}.°C^{-2})
CS	12.31	−18.41	−1.20	192.4	407.5	118.7	6.50	1.56	2.20
HC 180–0.5	5.42	−49.24	−1.67	288.8	442.3	153.5	22.29	3.85	5.90
HC 200–0.5	23.84	−57.56	−1.46	294.2	460.8	166.6	21.07	4.24	6.65
HC 220–0.5	6.87	−28.73	−1.33	291.3	484.3	193.0	9.30	2.03	3.38
HC 240–0.5	28.33	−13.73	−0.99	270.2	502.5	232.3	3.71	1.01	1.88
HC 200–2	16.40	−42.62	−1.44	279.4	464.2	184.8	16.94	3.28	5.45
HC 200–4	3.70	−47.13	−1.62	282.9	460.4	177.5	20.72	3.61	5.88

temperature of 460°C compared to the two HC produced at 200°C at a longer exposure time (2, 4 h), exhibit Tb temperatures of 464°C and 460°C, respectively. It can therefore be concluded that the prolonged exposure time of HTC has no significant effect on the combustion characteristics of the hydrochar, contrary to the effect of HTC temperatures that does improve the combustion performance of the HC [41]. The results of combustibility index (CCI), ignition index (Di), and flammability index (F) show that these three parameters decrease with increasing HTC temperature from 22.29 ($10^{-7}\%^2.min^{-2}.°C^{-3}$) to 3.71 ($10^{-7}\%^2.min^{-2}.°C^{-3}$), from 3.85 ($10^{-4}\%.min^{-1}.°C^{-2}$) to 1.01 ($10^{-4}\%.min^{-1}.°C^{-2}$) and from 5.90 (10–4%.$min^{-1}.°C^{-2}$) to 1.88 ($10^{-4}$ %.$min^{-1}.°C^{-2}$),respectively, at 180°C and 240°C. At lower HTC temperatures, CS hydrochars exhibit CCI values higher than those reported for lignite (1.52–6.75 ($10^{-7}\%^2.min^{-2}.°C^{-3}$)), while at higher temperatures, the CCI values fall within or below this range [42–44]. Based on these results, it can be concluded that HC200–0.5, with the highest values of

CCI, Di, and F, shows the best combustion performance and appears to be the most suitable hydrochar for use as fuel.

3.4. Surface morphology of CS and hydrochars

The effect of the HTC temperatures on the surface morphology of HC (for exposure time of 0.5 h) is shown on Fig. 4.

Sorghum has an orderly structure of well-connected lignocellulosic fibers, characteristic of its intact plant matrix. At 180°C, the hydrolysis of hemicelluloses and the breakdown of hydrogen bonds break the structure of the fibers, leading to isolated fragments [45]. At 200°C, partial lignin fusion and carbonization reactions promoted the formation of spheres, and recombined lignin microspheres or carbon aggregates [46]. At higher temperatures (220–240°C), complete depolymerization of cellulose and condensation of degradation products result in HC consisting of fine particles [47,48]. These transformations, consistent with studies on HTC, suggest a gradual loss of native structure in favor of amorphous materials whose specific surface area and reactivity could be increased[49,50].

3.5. Surface functional groups of contaminated sorghum and hydrochar

During HTC, CS is converted into HC, which is a rich carbon product, through chemical transformation. FTIR analysis was performed to examine the changes in organic functional groups of CS compared to the HC after HTC. The FTIR spectra of CS and HC produced at different temperatures (180–200–220 and 240°C) are shown in Fig. 5(a) and the FTIR spectra of CS and HC produced at different exposure times (0.5–2 and 4 h) are shown in Fig. 5(b). It can be observed that the FTIR spectrum of HC were different, which corresponded to changes in chemical components.

The CS and HC transmittance spectra are characterized by a peak at 3350 cm^{-1}, which remains at similar intensity across all four HTC temperatures (180–200–220–240°C). This peak is tuned to the O-H stretch vibration in the hydroxyl and carbonyl groups [51]. On the other hand, this peak becomes less intense with the increase in reaction temperature from 180 to 240°C and exposure time elongation from 0.5 h to 4 h, which is explained by the appearance of a dehydration reaction during the HTC of CS [52]. The (C-H) band at 2913 cm^{-1} refers to dehydration and partial aromatization of the CS during HTC [53]. This peak becomes more intense with the increase of temperature and exposure time. The transmittance peak at 1611 cm^{-1} corresponds to the stretching of C═O in ketone, amide and carboxylic groups [54]. This peak increases with the increasing temperature and longer exposure time, demonstrating the appearance of decarboxylation reaction. This augmentation in carboxyl groups may reduce the HMs removal from the hydrochar. Peaks at 1200–1150 cm^{-1} correspond to stretching C═C in aromatic groups and stretching C-O in lignin that decreases with increasing temperature and exposure time due to the decarboxylation of lignin [55]. The stretching of aliphatic ether C–O and alcohol C–O is related to peak 1050 cm^{-1}[56].

3.6. Liquid phase characterization and chemical composition

The liquid phase (Lp) of the HTC of CS has a dark brown color. Under the different operating conditions performed in this study, the pH and the conductivity of the HTC Lp remain constant at 3.96 ± 0.08 and 8.66 ± 0.23mS/cm, respectively. The Volume of Lp produced during the HTC of CS was around 445.41 ± 29.51 mL. The HTC of CS results in a liquid phase with a complex matrix of various organic compounds. Table 4 shows the quantified chemical compounds and the total organic carbon (TOC) in the HTC Lp of CS.

The TOC concentrations of HTC liquid phases vary between 9820 and 15810 mg/L, due to the presence of a wide range of organic compounds such as: furans, phenols, carboxylic acids. The TOC of the liquid phase decreases from 15810 to 10615 mg/L with an increasing temperature from 180 to 240°C. The same profile repeats for longer exposure times, ranging from 11682 to 9820 mg/L at 0.5 and 4 h, respectively. This trend suggests an acceleration of decarboxylation reactions of oligomers from lignin and carboxylic acids from holocellulose [57]. The HTC liquid phase of CS is a complex matrix with various organic compounds. The most common furfurals present in the HTC liquid phase are 2-Furaldehyde and 5-(Hydroxymethyl)-2-furaldehyde with a high concentration of 2001 and 790 mg/L at 180°C, respectively. The yield of these furfurals decreases with the increase of temperature; they most probably convert to organic acids at the higher temperatures 220 and 240°C [10]. Previous studies have indicated that organic acids derive from xylose, furfural, glucose and fructose [58–60]. The presence of carboxylic acids explains the constant acidic pH value of the HTC liquid phase namely 3.9. The most common carboxylic acids in our

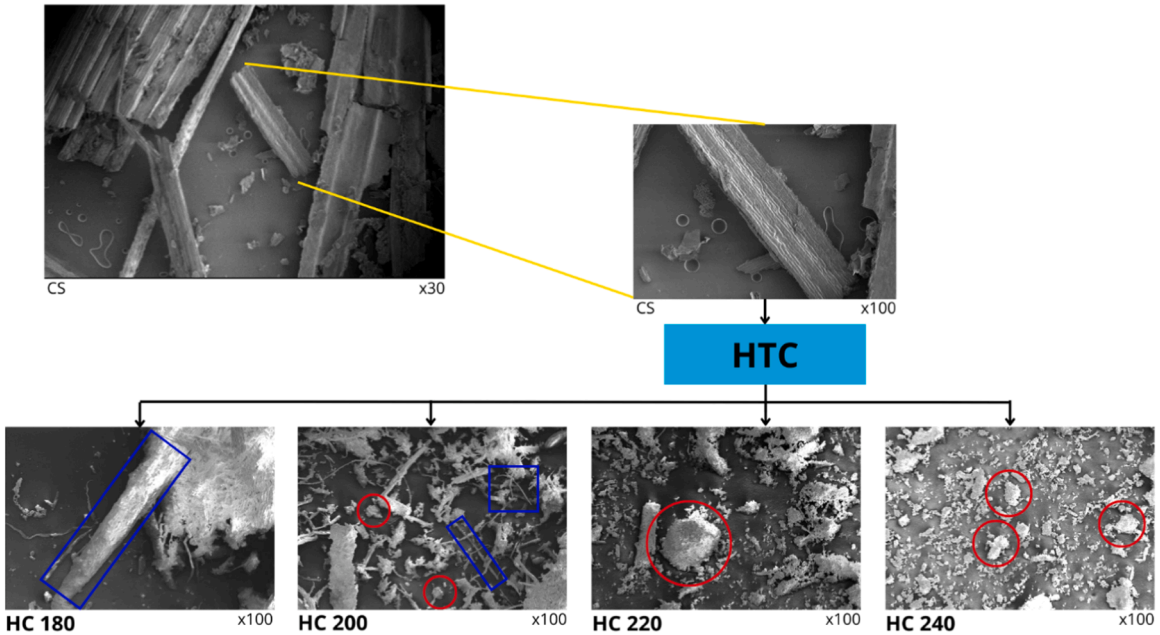

Fig. 4. Scanning Electron Microscopy images of CS and hydrochars at 180, 200, 220 and 240°C for 0.5 h.

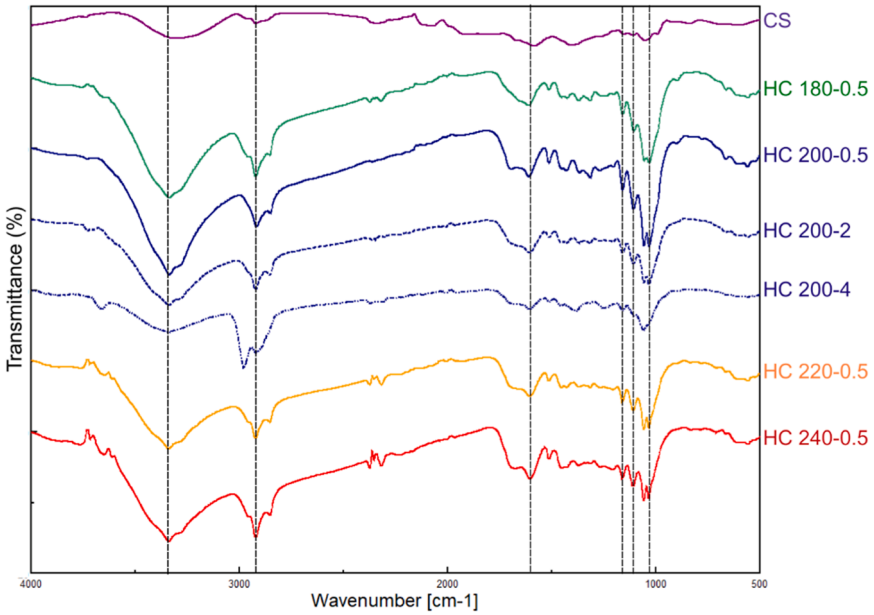

Fig. 5. FTIR spectra of CS and hydrochars; (a) Temperature effect (180–200–220 and 240°C); (b) Exposure time effect (0.5–2 and 4 h).

Table 4
TOC and the chemical composition of the HTC liquid phase of CS.

Compounds (mg/L)	Lp 180–0.5	Lp 200–0.5	Lp 220–0.5	Lp 240–0.5	Lp 200–2	Lp 200–4
TOC	15030 ± 0.07	11525 ± 0.18	10132 ± 0.66	10252 ± 0.10	10244 ± 0.33	9320 ± 0.00
2-Furaldehyde	2001 ± 2.60	1205 ± 10.55	365 ± 9.19	65 ± 2.15	643 ± 5.86	272 ± 3.59
3-Furaldehyde	30 ± 0.30	30 ± 0.09	30 ± 0.00	30 ± 0.00	30 ± 0.00	30 ± 0.00
4-(2-Furyl)−3-buten−2-one	12 ± 0.06	10 ± 0.09	15 ± 0.60	11 ± 1.09	12 ± 0.11	11 ± 1.41
4-Hydroxybenzoic acid	33 ± 0.81	19 ± 0.95	5 ± 0.34	5 ± 0.68	7 ± 0.81	6 ± 1.05
5-(Hydroxymethyl)−2-furaldehyde	790 ± 4.43	750 ± 0.25	300 ± 0.05	100 ± 0.07	430 ± 3.58	251 ± 0.12
5-Methyl−2-furaldehyde	41 ± 0.11	33 ± 0.07	22 ± 0.02	13 ± 0.04	25 ± 0.07	16 ± 0.00
Diacetone alcohol	1500 ± 0.66	250 ± 0.04	500 ± 10.37	500 ± 0.12	600 ± 0.02	400 ± 1.19
Guaiacol	14 ± 0.13	27 ± 0.18	33 ± 0.95	52 ± 0.41	2 ± 0.56	32 ± 0.53
Phenol	50 ± 0.02	50 ± 0.12	50 ± 0.03	50 ± 0.04	50 ± 0.04	50 ± 0.00
Vanilline	22 ± 0.20	22 ± 0.20	19 ± 0.18	17 ± 0.15	20 ± 0.15	16 ± 0.20
Vanillic acid	15 ± 0.05	15 ± 0.05	15 ± 0.05	15 ± 0.05	15 ± 0.05	15 ± 0.05
Benzoic acid	40 ± 0.00	40 ± 0.00	40 ± 0.00	40 ± 0.00	40 ± 0.00	40 ± 0.00
Acetic acid	3005 ± 5.20	3921 ± 21.10	4518 ± 18.38	5104 ± 4.31	4012 ± 11.72	4207 ± 7.17
Citric acid	281 ± 0.59	49 ± 0.18	10 ± 0.00	10 ± 0.00	10 ± 0.00	10 ± 0.00
Formic acid	1191 ± 8.87	1400 ± 0.17	1021 ± 20.75	532 ± 2.18	1207 ± 7.16	1097 ± 2.83
Lactic acid	249 ± 1.32	342 ± 1.91	569 ± 1.20	969 ± 1.36	392 ± 1.61	442 ± 2.10
Malic acid	242 ± 1.63	229 ± 0.50	161 ± 0.69	95 ± 0.13	200 ± 0.22	188 ± 2.37
Oxalic acid	58 ± 0.13	55 ± 0.14	55 ± 0.10	36 ± 0.08	48 ± 0.15	48 ± 0.23
Propionic acid	24 ± 0.22	45 ± 0.08	65 ± 0.04	84 ± 0.24	54 ± 0.05	63 ± 0.00
Pyruvic acid	660 ± 0.26	480 ± 0.36	208 ± 1.91	131 ± 0.81	251 ± 1.11	191 ± 1.07
Valeric acid	22 ± 0.04	16 ± 0.24	13 ± 0.06	10 ± 0.07	11 ± 0.09	10 ± 0.00

liquid samples are acetic acid, formic acid, pyruvic acid, and malic acid. The concentration of acetic acid increased from 3005 to 5104 mg/L with the increase of temperature (from 180 to 240°C) and from 3921 to 4207 mg/L with the elongation of exposure time (from 0.5 to 4 h). This can be explained by the production of acetic acid not just related to the decomposition of sugars but also via the decarboxylation of lactic acid to acetaldehyde and the subsequent oxidation of acetaldehyde to acetic acid [61]. A longer carbonization time also promotes the breakdown of intermediates (furfurals and alcohols) into gaseous compounds (CO_2, CO, CH_4 et H_2) [57]. To perform a mass balance and to better evaluate the effect of temperature and exposure time on the distribution of the various compounds in the liquid phase of the HTC, the concentrations of organic compounds are converted from mg/L to molC/L. The percentage of undetected compounds are calculated based on the difference between the carbon concentration (molC/L) of TOC and the organic compounds in the HTC Lp. Fig. 6 shows the distribution of the most abundant chemical compounds present in the liquid phase which are: carboxylic acid, furfurals, diacetone alcohol, phenols, and the undetected compounds.

Most of the liquid phase produced at 240°C is composed of carboxylic acids, accounting for 48.53 %. This result aligns with the earlier observation that higher temperatures and longer exposure times promote the conversion of furfurals into carboxylic acids by rearrangement. As the temperature increases, the percentage of furfurals decreases, demonstrating an inverse relationship with the rising percentage of carboxylic acids.

3.7. *Removal efficiency of heavy metals from contaminated sorghum*

The concentration of HMs within hydrochar can either enhance or restrict its potential applications as solid biofuel. Fig. 7 illustrates the effects of hydrothermal temperature (at a fixed exposure time of 0.5 h) and exposure time (at a constant temperature of 200°C) on the removal efficiency of seven major metal elements: Al, Cd, Fe, Mn, Ni, Pb, and Zn.

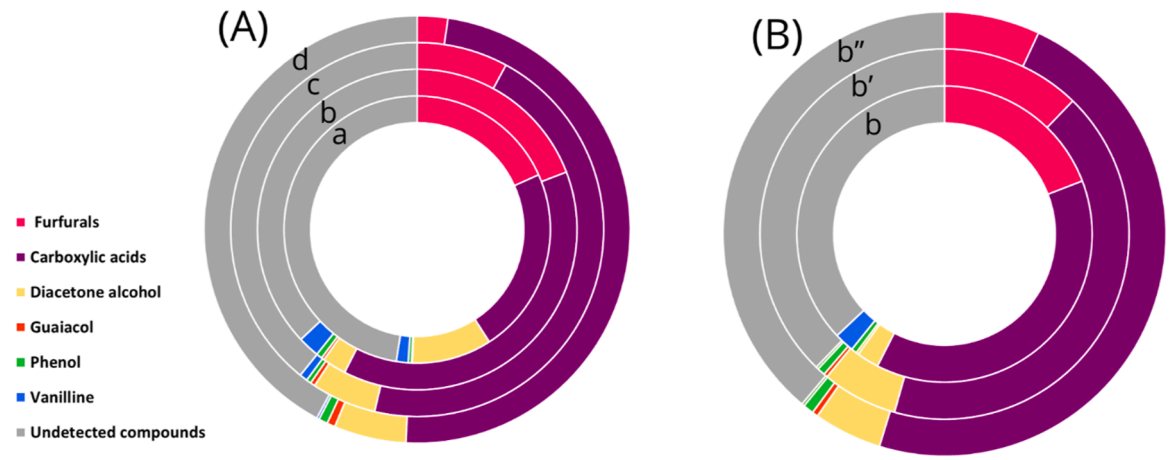

Fig. 6. Effect of temperature (A) (with exposure time:0.5 h; a: 180°C; b:200°C; c:220°C and d:240°C) and exposure time (B) (with Temperature: 200°C; b:0.5 h; b':2 h and b'':4 h) on the percentage distribution of organic chemical compounds in HTC Lp.

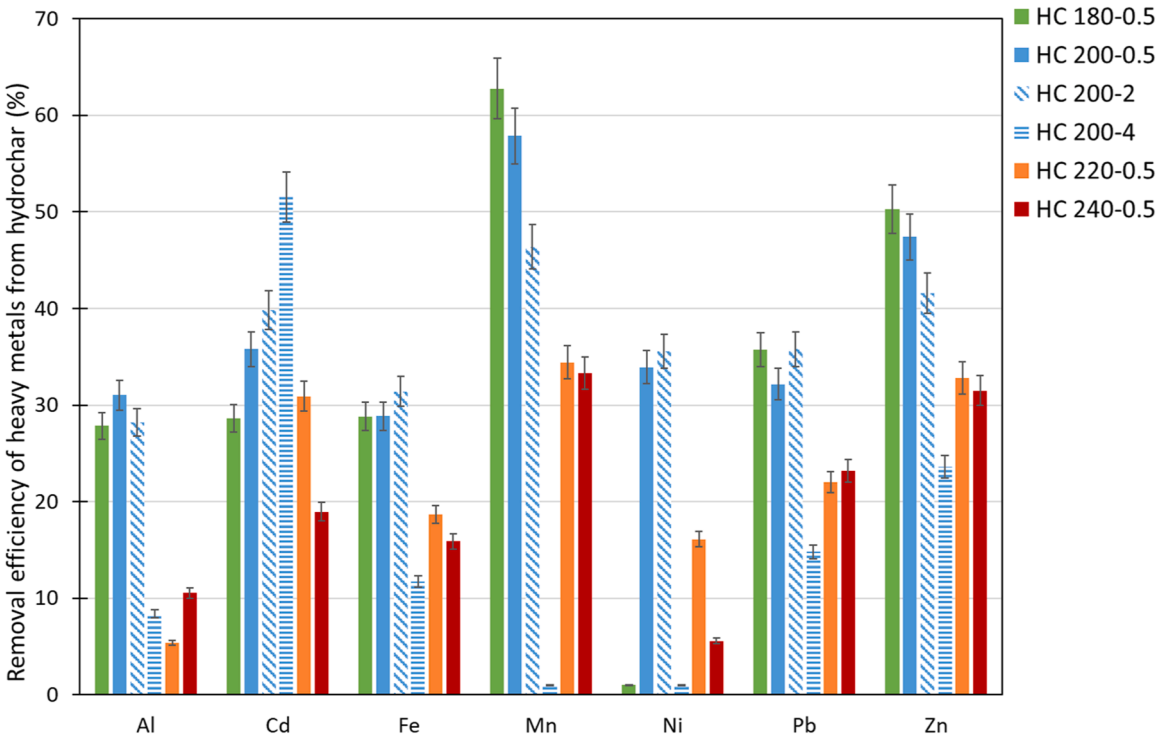

Fig. 7. Effect of temperature and exposure time on heavy metals removal efficiency from contaminated sorghum.

The removal of HMs from HC by HTC is temperature and exposure time dependent. At moderate temperatures (0.5 h at 180–200°C), Al, Cd, Fe, and Pb removal efficiencies are about 30 %, while Mn (~60 %) and Zn (~50 %) show higher removal rates. Ni is still relatively unaffected (1–2 % at 180°C), potentially due to its strong interaction with the organic matter or the mineral phases of the biomass [62]. The greater mobility of Mn and Zn may be attributed to their tendency to form soluble hydroxides or organometallic complexes during HTC [63]. When the temperature increases to 220–240°C (0.5 h), removal efficiencies decline for most metals (10–20 %), except Mn and Zn (~30 %). This suggests that higher temperatures promote HMs re-stabilization in the hydrochar matrix. As discussed in Sections 3–5, increasing temperature creates aromatic structures and oxygen-containing functional groups (e.g., carboxyl, phenolic) that can re-adsorb metals [64]. Extending the treatment time at 200°C reveals that 2 h maintains the removal efficiency similar to the 0.5 h treatment, but the 4 h exposure reduces the extraction for Al, Fe, Mn, Ni, Pb, and Zn. This observation aligns with studies showing that prolonged HTC enhances carbonization, leading to metal encapsulation in the HC's porous structure, thus limiting inorganic elements leaching [50]. Temperature of 200°C and the exposure times 0.5–2 h were concluded to be favorable conditions.

Comparing the concentrations of Cd, Ni, Pb, and Zn in the hydrochar and the upper limit of the allowed concentrations according to the ISO 17225:2014 standard for solid biofuels (Table 5) it becomes obvious that the proposed operating conditions (200°C for 0.5–2 h) are insufficient for effective decontamination of CS [65,66]. Therefore, optimizing the HTC process of CS is necessary, potentially by incorporating additives such as acids to enhance metal removal. On the other hand, the concentration of HMs in the HTC liquid phase of contaminated sorghum remains significantly higher than the safe limits established by the World Health Organization (WHO) for wastewater [67]. This finding highlights the need for appropriate post-treatment such as advanced

Table 5
Heavy metals content in HTC products of CS compared to regulatory standards.

	HC 200–0.5 (mg/kg)	HC 200–2 (mg/kg)	Biofuel standard ISO 17225:2014 (mg/kg) [65,66]	Lp 200–0.5 (mg/L)	Lp 200–2 (mg/L)	WHO standard for wastewater (mg/L) [67]
Al	1252 ± 248.36	1430 ± 370.35	_	0.56 ± 0.05	0.42 ± 0.02	5.00
Cd	18 ± 0.83	19 ± 1.30	≤ 0.5	0.33 ± 0.00	0.31 ± 0.07	0.02
Fe	907 ± 192.33	960 ± 140.0	_	11.43 ± 0.56	12.03 ± 2.53	5.00
Mn	37 ± 2.89	52 ± 1.16	_	6.38 ± 0.12	6.29 ± 0.10	1.00
Ni	6 ± 0.93	6 ± 0.83	≤ 10.0	0.11 ± 0.03	0.12 ± 0.01	0.20
Pb	206 ± 23.48	214 ± 35.76	≤ 10.0	0.75 ± 0.23	0.59 ± 0.22	0.05
Zn	225 ± 24.73	275 ± 15.35	≤ 100.0	17.54 ± 0.45	16.06 ± 0.06	0.50

oxidation processes, adsorption, chemical precipitation, or disposal strategies to mitigate potential environmental and health risks associated with HTC liquid phase.

3.8. Phytotoxicity evaluation of HTC liquid phase

Completing the HMs and TOC results, the phytotoxicity test was performed to evaluate the phytotoxicity impact of the HTC liquid phase of CS. According to germination index (GI) percentages, compounds are categorized as follows: high phytotoxicity for GI values below 50 %, moderate phytotoxicity for GI values between 50 % and 80 %, and no phytotoxicity for GI values above 80 % [68]. Table 6 shows the GI of HTC liquid phase, where Raw stands for the undiluted sample.

In this case, the undiluted HTC liquid phase of CS shows very high phytotoxicity because the GI is 0 %. The very low germination index (GI) of 12–16 % is attributed to the presence of toxic compounds in the HTC liquid phase. These include organic acids (e.g., acetic, and formic acids) and furans/phenolics (e.g., phenol and guaiacol), which are byproducts of sorghum degradation during HTC. Phenolic compounds can disrupt enzyme activity, membrane permeability, and hormonal regulation in seeds even at low concentrations (10–50 mg/L), can reduce the GI by up to 50 % [69]. Carboxylic acids contribute to a significant pH drop (around pH=4 in HTC Lp), which can directly inhibit germination. At higher concentrations, these acids can denature proteins and lyse cellular membranes [70]. In addition, the presence of HMs in the HTC Lp can further impair germination and seedling growth by inducing oxidative stress, inhibiting enzymes, and damaging membranes [71,72]. The GI of the diluted HTC Lp by ten is improved to 42 %, this suggests that the toxic compounds (furans, phenolics, acids and HMs) lose their harmful impact when their concentration is reduced.

3.9. Discussion

The results of this research highlight the complexity of the valorization of CS by HTC, a process that aims, on the one hand, to optimize the energy properties of HC, and, on the other hand, ensure effective disposal of HMs to meet the requirements of environmental standards. The favorable combustion profile of the HC200–0.5 sample, combining good combustion index (CCI), high delayed ignition temperature (ΔT), and reduced processing time, positions it as the best candidate for use as a solid biofuel. However, the HMs analysis reveals that residual concentrations of Cd, Ni, Pb and Zn in hydrochar exceed the limits set by ISO 17225:2014 [65], making this material still non-compliant without further optimization. In parallel, the liquid phase generated during the HTC process also poses a major environmental challenge. Although the transfer of HMs to this phase seems to improve its quality as a solid biofuel, the concentrations of HMs in the liquid are well above the World Health Organization (WHO) recommended thresholds for wastewater [67]. This excludes the possibility of direct release into the environment without appropriate treatment. Thus, the effectiveness of the HTC process in treating contaminated sorghum cannot be assessed solely through the quality of the solid product. It is imperative to adopt an integrated approach, considering the rigorous management of the liquid phase. Post-treatment strategies such as chemical precipitation, adsorption of specific materials, advanced oxidation processes or containment and targeted recovery solutions are essential to reduce the phyto-toxicological risks associated with this phase and to ensure compliance with the international effluent discharge standards. Furthermore, the element-specific behavior of HMs suggests that standardized operating conditions are not sufficient for effective removal. Though HTC holds great potential for the energy recovery of contaminated biomass, its environmental sustainability is highly dependent on integrated management of the secondary products (liquid phase). This study illustrates that technological optimization, and a system perspective are necessary to make this process viable and safe at large scale.

Table 6
Germination index percentages of HTC liquid phase.

	Raw	Dilution × 2	Dilution × 5	Dilution × 10
GI (%)	0	12,44 ± 1.33	16,59 ± 0.80	42,32 ± 1.12

4. Conclusions

This study provides new insights into the potential of hydrothermal carbonization (HTC) as a sustainable method for converting HMs contaminated sorghum into a valuable solid biofuel. Among the conditions tested, hydrochar produced at 200°C for 0.5 h (HC200–0.5) emerges as the best candidate due to its favorable combustion performance and comparatively lower HMs content (30–60 % HMs removed). One of the most significant contributions of the present work is the identification of this specific condition as an optimal balance between contaminant reduction and energy recovery. However, the results also indicate that current HTC conditions are still not sufficient for complete removal. This highlights the need for further process optimization, particularly through the integration of additives to enhance metal mobility and removal. Furthermore, this study addresses the often-overlooked environmental implications of the HTC liquid by-product. The high concentrations of both organic matter and HMs, coupled with strong phytotoxic effects, clearly indicate that the liquid phase cannot be discharged without prior treatment. To date, only a few studies have addressed simultaneously the aspects of combustion performance, HMs behavior, and HTC Lp phytotoxicity under different HTC conditions for contaminated sorghum conversion, proposing this work as a valuable contribution to the field. Further research should explore the use of additives, catalysts, and process modifications to improve metal extraction efficiency. In addition, designing scalable and cost-effective treatment processes for the HTC liquid phase is essential to ensure the environmental sustainability of this valorization pathway, an area in which this study lays important groundwork and something continued work is still being conducted on.

CRediT authorship contribution statement

Mathilde Mercier: Supervision. **Lydia Fryda:** Supervision. **Hayet Djelal:** Supervision. **MEHREZ Karima:** Writing – original draft. **Nathalie Leblanc:** Supervision. **Rian Visser:** Supervision. **Heather**

Wray: Supervision. **Abdoulaye Kane:** Supervision.

Funding

This work was supported by Unilasalle Ecole des Métiers de l'Environnement-Brittany France and the Department of Energy Transition, Dutch Institute of Applied Research (TNO), Westerduinweg 3, 1755 LE Petten, The Netherlands.

Declaration of Competing Interest

The authors declare that they have no known competing financial interests or personal relationships that could have appeared to influence the work reported in this paper.

Data Availability

Data will be made available on request.

References

[1] A. Sharma, A.S. Grewal, D. Sharma, A.L. Srivastav, Chapter 3 - Heavy metal contamination in water: consequences on human health and environment, in: S. K. Shukla, S. Kumar, S. Madhav, P.K. Mishra (Eds.), Metals in Water, Elsevier, 2023, pp. 39–52.
[2] S. Mitra, A.J. Chakraborty, A.M. Tareq, et al., Impact of heavy metals on the environment and human health: novel therapeutic insights to counter the toxicity, J. King Saud. Univ. Sci. 34 (2022) 101865, https://doi.org/10.1016/j.jksus.2022.101865.
[3] M. Jaishankar, T. Tseten, N. Anbalagan, et al., Toxicity, mechanism and health effects of some heavy metals, Inter. Toxicol. 7 (2014) 60–72, https://doi.org/10.2478/intox-2014-0009.
[4] M. Edelstein, M. Ben-Hur, Heavy metals and metalloids: sources, risks and strategies to reduce their accumulation in horticultural crops, Sci. Hortic. 234 (2018) 431–444, https://doi.org/10.1016/j.scienta.2017.12.039.
[5] K.A. Alaboudi, B. Ahmed, G. Brodie, Phytoremediation of Pb and Cd contaminated soils by using sunflower (*Helianthus annuus*) plant, Ann. Agric. Sci. 63 (2018) 123–127, https://doi.org/10.1016/j.aoas.2018.05.007.
[6] V. Angelova, Phytoremediation potential of miscanthus X giganteus in soil contaminated with heavy metals, Earth Obs. (2020).
[7] S.V. Gorelova, A.P. Kolbas, A.Yu Muratova, et al., Prospects for the use of sorghum bicolor for phytoremediation of soils contaminated with heavy metals in temperate climates, in: L. Newman, A.A. Ansari, S.S. Gill, et al. (Eds.), Phytoremediation: Management of Environmental Contaminants, 7, Springer International Publishing, Cham, 2023, pp. 263–301.
[8] A.H.A. Khan, A. Kiyani, M. Santiago-Herrera, et al., Sustainability of phytoremediation: Post-harvest stratagems and economic opportunities for the produced metals contaminated biomass, in: J Environ Manage, 326, 2023, https://doi.org/10.1016/j.jenvman.2022.116700.
[9] Y. Chai, M. Bai, A. Chen, et al., Thermochemical conversion of heavy metal contaminated biomass: fate of the metals and their impact on products, Sci. Total Environ. 822 (2022) 153426, https://doi.org/10.1016/j.scitotenv.2022.153426.
[10] M.T. Reza, J. Andert, B. Herklotz, et al., Review article: hydrothermal carbonization of biomass for energy and crop production, Appl. Bioenergy 1 (2014), https://doi.org/10.2478/apbi-2014-0001.
[11] A.L. Pauline, K. Joseph, Hydrothermal carbonization of organic wastes to carbonaceous solid fuel – a review of mechanisms and process parameters, Fuel 279 (2020) 118472, https://doi.org/10.1016/j.fuel.2020.118472.
[12] X. Cui, M. Lu, M.B. Khan, et al., Hydrothermal carbonization of different wetland biomass wastes: Phosphorus reclamation and hydrochar production, Waste Manag 102 (2020) 106–113, https://doi.org/10.1016/j.wasman.2019.10.034.
[13] S. Li, W. Zhang, REE recovery and hydrochar production from a hyperaccumulator by microwave-assisted hydrothermal carbonization, Min. Eng. 208 (2024) 108595, https://doi.org/10.1016/j.mineng.2024.108595.
[14] D. Kim, K. Yoshikawa, K.Y. Park, Characteristics of biochar obtained by hydrothermal carbonization of cellulose for renewable energy, Energies 8 (2015) 14040–14048, https://doi.org/10.3390/en81212412.
[15] K. Czerwińska, M. Śliz, M. Wilk, Hydrothermal carbonization process: fundamentals, main parameter characteristics and possible applications including an effective method of SARS-CoV-2 mitigation in sewage sludge. A review, Renew. Sustain Energy Rev. 154 (2022) 111873, https://doi.org/10.1016/j.rser.2021.111873.
[16] J. Zhang, Y. Wang, X. Wang, et al., Hydrothermal conversion of Cd/Zn hyperaccumulator (Sedum alfredii) for heavy metal separation and hydrochar production, J. Hazard Mater. 423 (2022) 127122, https://doi.org/10.1016/j.jhazmat.2021.127122.
[17] Z. Wang, P. Luo, X. Zha, et al., Overview assessment of risk evaluation and treatment technologies for heavy metal pollution of water and soil, J. Clean. Prod. 379 (2022) 134043, https://doi.org/10.1016/j.jclepro.2022.134043.
[18] E. Di Iorio, L. Circelli, R. Angelico, et al., Environmental implications of interaction between humic substances and iron oxide nanoparticles: a review, Chemosphere 303 (2022) 135172, https://doi.org/10.1016/j.chemosphere.2022.135172.
[19] H. Jeong, E. Byeon, D.-H. Kim, et al., Heavy metals and metalloid in aquatic invertebrates: a review of single/mixed forms, combination with other pollutants, and environmental factors, Mar. Pollut. Bull. 191 (2023) 114959, https://doi.org/10.1016/j.marpolbul.2023.114959.
[20] K. Mehrez, L. Fryda, R. Visser, et al., Hydrothermal processes of contaminated biomass: fate of heavy metals and liquid effluent valorization, Biomass. Convers. Biorefinery (2024), https://doi.org/10.1007/s13399-024-06023-0.
[21] S. Li, B. Ji, W. Zhang, A review on the thermochemical treatments of biomass: Implications for hydrochar production and rare earth element recovery from hyperaccumulators, Chemosphere 342 (2023) 140140, https://doi.org/10.1016/j.chemosphere.2023.140140.
[22] W. Su, X. Li, H. Zhang, et al., Migration and transformation of heavy metals in hyperaccumulators during the thermal treatment: a review, Environ. Sci. Pollut. Res. 28 (2021) 47838–47855, https://doi.org/10.1007/s11356-021-15346-8.
[23] S. Jiang, J. Sun, G. Tong, et al., Emerging disposal technologies of harmful phytoextraction biomass (HPB) containing heavy metals: a review, Chemosphere 290 (2022) 133266, https://doi.org/10.1016/j.chemosphere.2021.133266.
[24] E. Tristán, M. Ramsey, I. Thornton, , 1999, Spatially resolved hazard and exposure assessments. Geochem Atlas Lavrion Urban Area Environ Prot Plan Proj "Soil Rehabil Munic Lavrion" EU LIFE Programme Contract No 93:311–349.
[25] J. Luo, Z. Lin, T. Xie, et al., Valorization of kitchen waste hydrolysis residue for green solid fuel application: Conversion mechanism and fuel characteristics, Fuel 375 (2024) 132556, https://doi.org/10.1016/j.fuel.2024.132556.
[26] R. Ma, S. Fakudze, S. Liu, et al., Surfactants/citric acid catalyzed hydrothermal carbonization of pomelo peel for solid fuels: conversion mechanism and combustion performance, Fuel 342 (2023) 127762, https://doi.org/10.1016/j.fuel.2023.127762.
[27] C. Wei, Z. Yu, X. Zhang, X. Ma, Co-combustion behavior of municipal solid waste and food waste anaerobic digestates: combustion performance, kinetics, optimization, and gaseous products, J. Environ. Chem. Eng. 9 (2021) 106028, https://doi.org/10.1016/j.jece.2021.106028.
[28] Z. Liu, A. Quek, S. Kent Hoekman, et al., Thermogravimetric investigation of hydrochar-lignite co-combustion, Bioresour. Technol. 123 (2012) 646–652, https://doi.org/10.1016/j.biortech.2012.06.063.
[29] G.K. Parshetti, S. Kent Hoekman, R. Balasubramanian, Chemical, structural and combustion characteristics of carbonaceous products obtained by hydrothermal carbonization of palm empty fruit bunches, Bioresour. Technol. 135 (2013) 683–689, https://doi.org/10.1016/j.biortech.2012.09.042.
[30] Y. Shen, A review on hydrothermal carbonization of biomass and plastic wastes to energy products, Biomass. Bioenergy 134 (2020) 105479, https://doi.org/10.1016/j.biombioe.2020.105479.
[31] E. García-Bordejé, E. Pires, J.M. Fraile, Parametric study of the hydrothermal carbonization of cellulose and effect of acidic conditions, Carbon 123 (2017) 421–432, https://doi.org/10.1016/j.carbon.2017.07.085.
[32] M. Lucian, M. Volpe, L. Gao, et al., Impact of hydrothermal carbonization conditions on the formation of hydrochars and secondary chars from the organic fraction of municipal solid waste, Fuel 233 (2018) 257–268, https://doi.org/10.1016/j.fuel.2018.06.060.
[33] S. Sattasathuchana, J. Parnthong, S. Youngian, et al., Energy efficiency of bio-coal derived from hydrothermal carbonized biomass: assessment as sustainable solid fuel for municipal biopower plant, Appl. Therm. Eng. 221 (2023) 119789, https://doi.org/10.1016/j.applthermaleng.2022.119789.
[34] M. Santos Santana, R. Pereira Alves, W.M. da Silva Borges, et al., Hydrochar production from defective coffee beans by hydrothermal carbonization, Bioresour. Technol. 300 (2020) 122653, https://doi.org/10.1016/j.biortech.2019.122653.
[35] S. Wu, Q. Wang, D. Cui, et al., Evaluation of fuel properties and combustion behaviour of hydrochar derived from hydrothermal carbonisation of agricultural wastes, J. Energy Inst. 108 (2023) 101209, https://doi.org/10.1016/j.joei.2023.101209.
[36] K. Tekin, S. Karagöz, S. Bektaş, A review of hydrothermal biomass processing, Renew. Sustain Energy Rev. 40 (2014) 673–687, https://doi.org/10.1016/j.rser.2014.07.216.
[37] T. Wang, Y. Zhai, Y. Zhu, et al., A review of the hydrothermal carbonization of biomass waste for hydrochar formation: process conditions, fundamentals, and physicochemical properties, Renew. Sustain Energy Rev. 90 (2018) 223–247, https://doi.org/10.1016/j.rser.2018.03.071.
[38] K.Y. Park, K. Lee, D. Kim, Characterized hydrochar of algal biomass for producing solid fuel through hydrothermal carbonization, Bioresour. Technol. 258 (2018) 119–124, https://doi.org/10.1016/j.biortech.2018.03.003.
[39] J. Li, M.C. Paul, P.L. Younger, et al., Prediction of high-temperature rapid combustion behaviour of woody biomass particles, Fuel 165 (2016) 205–214, https://doi.org/10.1016/j.fuel.2015.10.061.
[40] M.T. Reza, E. Rottler, L. Herklotz, B. Wirth, Hydrothermal carbonization (HTC) of wheat straw: influence of feedwater pH prepared by acetic acid and potassium hydroxide, Bioresour. Technol. 182 (2015) 336–344, https://doi.org/10.1016/j.biortech.2015.02.024.
[41] D. Cui, B. Zhang, S. Wu, et al., From sewage sludge and lignocellulose to hydrochar by co-hydrothermal carbonization: mechanism and combustion characteristics, Energy 305 (2024) 132414, https://doi.org/10.1016/j.energy.2024.132414.
[42] Z. Xiao, S. Wang, M. Luo, J. Cai, Combustion characteristics and synergistic effects during co-combustion of lignite and lignocellulosic components under oxy-fuel condition, Fuel 310 (2022) 122399, https://doi.org/10.1016/j.fuel.2021.122399.

[43] Y. Dai, M. Sun, H. Fang, et al., Co-combustion of binary and ternary blends of industrial sludge, lignite and pine sawdust via thermogravimetric analysis: thermal behaviors, interaction effects, kinetics evaluation, and artificial neural network modeling, Renew. Energy 220 (2024) 119610, https://doi.org/10.1016/j.renene.2023.119610.
[44] H. Zhan, X. Zhuang, S. Zhang, et al., Evaluation on the enhanced solid biofuel from co-hydrothermal carbonization of pharmaceutical biowastes with lignite, Fuel 318 (2022) 123626, https://doi.org/10.1016/j.fuel.2022.123626.
[45] A. Funke, F. Ziegler, Hydrothermal carbonization of biomass: a summary and discussion of chemical mechanisms for process engineering, Biofuels Bioprod. Bioref. 4 (2010) 160–177, https://doi.org/10.1002/bbb.198.
[46] C. Falco, N. Baccile, M.-M. Titirici, Morphological and structural differences between glucose, cellulose and lignocellulosic biomass derived hydrothermal carbons, Green. Chem. 13 (2011) 3273–3281, https://doi.org/10.1039/C1GC15742F.
[47] G.K. Parshetti, S. Kent Hoekman, R. Balasubramanian, Chemical, structural and combustion characteristics of carbonaceous products obtained by hydrothermal carbonization of palm empty fruit bunches, Bioresour. Technol. 135 (2013) 683–689, https://doi.org/10.1016/j.biortech.2012.09.042.
[48] S.K. Hoekman, A. Broch, C. Robbins, Hydrothermal carbonization (HTC) of lignocellulosic biomass, Energy Fuels 25 (2011) 1802–1810, https://doi.org/10.1021/ef101745n.
[49] J.O. Ighalo, F.C. Akaeme, J. Georgin, et al., Biomass hydrochar: a critical review of process chemistry, synthesis methodology, and applications, Sustainability 17 (2025) 1660, https://doi.org/10.3390/su17041660.
[50] H.S. Kambo, A. Dutta, A comparative review of biochar and hydrochar in terms of production, physico-chemical properties and applications, Renew. Sustain. Energy Rev. 45 (2015) 359–378, https://doi.org/10.1016/j.rser.2015.01.050.
[51] G. Zhao, G. Kuang, Y. Wang, et al., Effect of steam explosion on physicochemical properties and fermentation characteristics of sorghum (*Sorghum bicolor* (L.) Moench), LWT 129 (2020) 109579, https://doi.org/10.1016/j.lwt.2020.109579.
[52] K. Nakason, B. Panyapinyopol, V. Kanokkantapong, et al., Characteristics of hydrochar and liquid fraction from hydrothermal carbonization of cassava rhizome, J. Energy Inst. 91 (2018) 184–193, https://doi.org/10.1016/j.joei.2017.01.002.
[53] A. Kruse, T.A. Zevaco, Properties of hydrochar as function of feedstock, reaction conditions and post-treatment, Energies 11 (2018) 674, https://doi.org/10.3390/en11030674.
[54] S. Yoshimoto, N. Luthfi, K. Nakano, et al., Effects of potassium on hydrothermal carbonization of sorghum bagasse, Bioresour. Bioprocess 10 (2023) 24, https://doi.org/10.1186/s40643-023-00645-4.
[55] P. Gao, Y. Zhou, F. Meng, et al., Preparation and characterization of hydrochar from waste eucalyptus bark by hydrothermal carbonization, Energy 97 (2016) 238–245, https://doi.org/10.1016/j.energy.2015.12.123.
[56] R. Thandavamoorthy, Y. Devarajan, N. Kaliappan, Antimicrobial, function, and crystalline analysis on the cellulose fibre extracted from the banana tree trunks, Sci. Rep. 13 (2023) 15301, https://doi.org/10.1038/s41598-023-42160-8.
[57] M. Heidari, A. Dutta, B. Acharya, S. Mahmud, A review of the current knowledge and challenges of hydrothermal carbonization for biomass conversion, J. Energy Inst. 92 (2019) 1779–1799, https://doi.org/10.1016/j.joei.2018.12.003.
[58] N. Paksung, Y. Matsumura, Decomposition of xylose in sub- and supercritical water, Ind. Eng. Chem. Res. 54 (2015) 7604–7613, https://doi.org/10.1021/acs.iecr.5b01623.
[59] J. Poerschmann, B. Weiner, R. Koehler, F.-D. Kopinke, Hydrothermal carbonization of glucose, fructose, and xylose—identification of organic products with medium molecular masses, ACS Sustain Chem. Eng. 5 (2017) 6420–6428, https://doi.org/10.1021/acssuschemeng.7b00276.
[60] F.S. Asghari, H. Yoshida, Kinetics of the decomposition of fructose catalyzed by hydrochloric acid in subcritical water: formation of 5-hydroxymethylfurfural, levulinic, and formic acids, Ind. Eng. Chem. Res 46 (2007) 7703–7710, https://doi.org/10.1021/ie061673e.
[61] T.M. Aida, A. Ikarashi, Y. Saito, et al., Dehydration of lactic acid to acrylic acid in high temperature water at high pressures, J. Supercrit. Fluids 50 (2009) 257–264, https://doi.org/10.1016/j.supflu.2009.06.006.
[62] J.A. Libra, Kyoung S. Ro, Claudia Kammann, et al., Hydrothermal carbonization of biomass residuals: a comparative review of the chemistry, processes and applications of wet and dry pyrolysis, Biofuels 2 (2011) 71–106, https://doi.org/10.4155/bfs.10.81.
[63] Q. Lang, M. Chen, Y. Guo, et al., Effect of hydrothermal carbonization on heavy metals in swine manure: speciation, bioavailability and environmental risk, J. Environ. Manag. 234 (2019) 97–103, https://doi.org/10.1016/j.jenvman.2018.12.073.
[64] J. Li, J. Chen, S. Chen, Supercritical water treatment of heavy metal and arsenic metalloid-bioaccumulating-biomass, Ecotoxicol. Environ. Saf. 157 (2018) 102–110, https://doi.org/10.1016/j.ecoenv.2018.03.069.
[65] ISO E (2014) 17225–2: 2014-Solid Biofuels-Fuel Specifications and Classes Part 2: Graded Wood Pellets. Br Stand Inst Lond UK.
[66] ISO 17225–7 (2014) Solid Biofuels—Fuel Specifications and Classes—Part 7: Graded Non-Woody Briquettes.
[67] World Health Organization, Asbestos in Drinking Water: Background Document for Development of WHO Guidelines for Drinking-water Quality, World Health Organization, 2021.
[68] H. Zeghioud, N. Khellaf, A. Amrane, et al., Combining photocatalytic process and biological treatment for Reactive Green 12 degradation: optimization, mineralization, and phytotoxicity with seed germination, Environ. Sci. Pollut. Res. 28 (2021) 12490–12499, https://doi.org/10.1007/s11356-020-11282-1.
[69] O. Karatas, A. Khataee, D. Kalderis, Recent progress on the phytotoxic effects of hydrochars and toxicity reduction approaches, Chemosphere 298 (2022) 134357, https://doi.org/10.1016/j.chemosphere.2022.134357.
[70] Suppressive activity of volatile fatty acids and aromatic carboxylic acids on the germination of Monochoria vaginalis. https://www.tandfonline.com/doi/full/10.1080/1343943X.2021.1896953. Accessed 1 May 2025.
[71] M. Jamla, T. Khare, S. Joshi, et al., Omics approaches for understanding heavy metal responses and tolerance in plants, Curr. Plant Biol. 27 (2021) 100213, https://doi.org/10.1016/j.cpb.2021.100213.
[72] S.A. Ghuge, G.C. Nikalje, U.S. Kadam, et al., Comprehensive mechanisms of heavy metal toxicity in plants, detoxification, and remediation, J. Hazard Mater. 450 (2023) 131039, https://doi.org/10.1016/j.jhazmat.2023.131039.